MRI of neurodegeneration with brain iron accumulation

Stéphane Lehéricy, Emmanuel Roze, Cyril Goizet, Fanny Mochel

▶ **To cite this version:**

Stéphane Lehéricy, Emmanuel Roze, Cyril Goizet, Fanny Mochel. MRI of neurodegeneration with brain iron accumulation. Current Opinion in Neurology, 2020, 33 (4), pp.462-473. 10.1097/WCO.0000000000000844 . hal-02935202

HAL Id: hal-02935202

https://hal.sorbonne-universite.fr/hal-02935202

Submitted on 10 Sep 2020

HAL is a multi-disciplinary open access archive for the deposit and dissemination of scientific research documents, whether they are published or not. The documents may come from teaching and research institutions in France or abroad, or from public or private research centers.

L'archive ouverte pluridisciplinaire **HAL**, est destinée au dépôt et à la diffusion de documents scientifiques de niveau recherche, publiés ou non, émanant des établissements d'enseignement et de recherche français ou étrangers, des laboratoires publics ou privés.

REVIEW

OPEN

CURRENT OPINION

MRI of neurodegeneration with brain iron accumulation

Stéphane Lehéricy[a,b,c], Emmanuel Roze[a,h], Cyril Goizet[e,f], and Fanny Mochel[a,d,g]

Purpose of review

The diagnosis of neurodegeneration with brain iron accumulation (NBIA) typically associates various extrapyramidal and pyramidal features, cognitive and psychiatric symptoms with bilateral hypointensities in the globus pallidus on iron-sensitive magnetic resonance images, reflecting the alteration of iron homeostasis in this area. This article details the contribution of MRI in the diagnosis by summarizing and comparing MRI patterns of the various NBIA subtypes.

Recent findings

MRI almost always shows characteristic changes combining iron accumulation and additional neuroimaging abnormalities. Iron-sensitive MRI shows iron deposition in the basal ganglia, particularly in bilateral globus pallidus and substantia nigra. Other regions may be affected depending on the NBIA subtypes including the cerebellum and dentate nucleus, the midbrain, the striatum, the thalamus, and the cortex. Atrophy of the cerebellum, brainstem, corpus callosum and cortex, and white matter changes may be associated and worsen with disease duration. Iron deposition can be quantified using $R2^*$ or quantitative susceptibility mapping.

Summary

Recent MRI advances allow depicting differences between the various subtypes of NBIA, providing a useful analytical framework for clinicians. Standardization of protocols for image acquisition and analysis may help improving the detection of imaging changes associated with NBIA and the quantification of iron deposition.

Keywords

dystonia, iron, MRI, neurodegeneration with brain iron accumulation, pyramidal, quantitative susceptibility mapping, $R2^*$ mapping, susceptibility-weighted imaging

Downloaded from https://journals.lww.com/co-neurology by BhDMf5ePHKav1zEoum1tQfN4a+kJLhEZgbsIHo4XMi0hCywCX1AWnYQp/IlQrHD3cyta2a0wcihGsQl9JEIXvjZmtfj5BFMnGs8olIT GbH5I020Vn9tGsw== on 09/10/2020

INTRODUCTION

Neurodegeneration with brain iron accumulation (NBIA) is a clinical–radiological syndrome with multiple genetic causes [1▪▪]. The prevalence of NBIA is about 0.5/100 000 [1▪▪]. Age of onset varies from early childhood to midlife. The clinical picture is one of a variable combination of movement disorders (dystonia–parkinsonism, cerebellar ataxia) with a prominent orofacial involvement, pyramidal dysfunction, intellectual disability or cognitive deterioration, and psychiatric disorders. Other clinical features may include epilepsy, pigmentary retinopathy, optic atrophy, axonal neuropathy or diabetes. Death usually occurs early. These clinical manifestations are typically associated with marked bilateral hypointensities in the globus pallidus on iron-sensitive magnetic resonance (MR) images, reflecting the alteration of iron homeostasis in this area [1▪▪,2▪▪]. By the time, neurologic features are obvious, brain MRI almost always shows characteristic changes, although these changes may occasionally appear only later over the disease course. Conversely,

[a]Paris Brain Institute, Institut du Cerveau et de la Moelle épinière – ICM, INSERM U 1127, CNRS UMR 7225, Sorbonne Université, Team 'Movement Investigations and Therapeutics' (MOV'IT), [b]ICM, Centre de NeuroImagerie de Recherche – CENIR, [c]Department of Neuroradiology, Pitié-Salpêtrière hospital (AP-HP), Paris, [d]Department of Genetics, Pitié - Salpêtrière Hospital, Public Assistance - Paris Hospitals (AP-HP), Paris, [e]Reference Center for Rare 'Neurogenetic' Diseases, Department of Medical Genetics, Pellegrin Hospital, Bordeaux University Hospital, [f]Rare Diseases Laboratory: Genetics and Metabolism (MRGM), INSERM U1211, Bordeaux University, Bordeaux, France, [g]Reference Center for Neurometabolic diseases, Pitié -Salpêtrière Hospital, Paris and [h]Department of Neurology, Pitie-Salpetrire Hospital, Public Assistance - Paris Hospitals (AP-HP), Paris

Correspondence to Stéphane Lehéricy, MD, PhD, Institut du Cerveau et de la Moelle épinière – ICM, Hôpital Pitié-Salpêtrière, 47 Boulevard de l'Hôpital, 75651 Paris Cedex 13, France.
E-mail: stephane.lehericy@upmc.fr

Curr Opin Neurol 2020, 33:462–473

DOI:10.1097/WCO.0000000000000844

This is an open access article distributed under the terms of the Creative Commons Attribution-Non Commercial-No Derivatives License 4.0 (CCBY-NC-ND), where it is permissible to download and share the work provided it is properly cited. The work cannot be changed in any way or used commercially without permission from the journal.

KEY POINTS

- NBIA is a heterogeneous group of neurodegenerative diseases due to pathogenic variants in genes involved in iron metabolism, complex lipid metabolism, mitochondrial function, and autophagic processes.
- Iron-sensitive MRI sequences are crucial for the diagnosis of NBIA by showing reduced signal intensity in the basal ganglia primarily affecting the globus pallidus, whereas other regions, such as the substantia nigra, the red nucleus, the dentate nucleus and the striatum are more variably affected.
- In primary disorders of iron metabolism (aceruloplasminemia, neuroferritinopathy), MRI also shows widespread iron deposition in the thalamus, cerebellum and cortex.
- The diagnosis of NBIA relies upon careful analysis of brain MRI and clinical features followed by molecular analyses.

rare patients are asymptomatic despite typical bipallidal T2 and T2* hypointensity. Additional clinical or neuroimaging abnormalities can be seen depending on the underlying cause and the disease duration. The culprit genes, inheritance pattern, distinctive clinical features and biological markers are summarized in Table 1.

NBIA may be broken into two groups: primary disorders of iron metabolism constituting neuroferritinopathy and aceruloplasminemia and disorders in which alteration of iron homeostasis results from a neuronal dysfunction of another origin. These secondary causes of disturbed iron homeostasis within the brain constitute panthotenate kinase-associated neurodegeneration (PKAN), phospholipase A2 group VI-associated neurodegeneration (PLAN), fatty acid 2 hydroxylase-associated neurodegeneration (FAHN), mitochondrial membrane protein-associated neurodegeneration (MPAN), beta-propeller protein-associated neurodegeneration (BPAN), coenzyme A synthase protein-associated neurodegeneration (CoPAN), Woodhouse–Sakati syndrome and Kufor–Rakeb syndrome [2▪▪]. A brief overview of the metabolic pathways supposed to be involved is presented in Supplementary box 1, http://links.lww.com/CONR/A51. Other diseases may present a NBIA-like pattern including GM1 gangliosidosis, AP4-deficiency syndrome and pathogenic variants in *GTPBP2*, *DDHD1,* or *SCP2*. Typically, primary disorders of iron metabolism have an onset later in life and are characterized by more diffuse MRI abnormalities.

The suspicion of a NBIA should not only be based upon brain MRI showing bilateral hypointensities in the globus pallidus on iron-sensitive MR images. The clinical symptoms are critical to guide diagnosis (Table 1), which shall be confirmed by molecular analysis of the various causative genes. Indeed, alteration of iron homeostasis is not confined to NBIA, and ferroptosis may participate in neurodegeneration in a wide range of disorders [3▪▪]. In clinical practice, physicians can occasionally encounter patients with neurodegenerative diseases and MRI abnormalities reminiscent of that observed in NBIA. This has been reported in various diseases, including multiple system atrophy, progressive supranuclear palsy, corticobasal degeneration, Huntington disease, and dentatorubral-pallidolyusian atrophy [4].

Neuroferritinopathy causes an alteration of iron storage by ferritin polymers with a subsequent release of free iron and subsequent iron-mediated oxidation. Aceruloplasminemia causes a major decrease of ferroxidase activity preventing iron exportation by astrocytes and their binding of extracellular transferrin. Iron thus accumulates in astrocytes, and neurons suffer from iron starvation at early stages, and eventually from iron-mediated oxidation at later stages. Interestingly, secondary alterations of iron homeostasis are mostly linked to disorders of synthesis or remodelling of complex lipids [2▪▪].

The treatment of NBIA is primarily symptomatic and may include deep brain stimulation and botulinum toxin for dystonia [5]. Physiotherapy, occupational therapy speech therapy and swallowing rehabilitation are critical for these patients. There are no registered drug for preventing gradual deterioration over the course of the disease. However, a recent double blind placebo-controlled trial testing iron chelation with deferiprone in patients with PKAN showed a trend towards slowing disease progression [6▪]. More promising, a recent preclinical study recently demonstrated that 4′-phosphopantetheine corrects coenzyme A, iron and dopamine metabolic defects in a mouse model of PKAN [7]. Survival of the severely disabled patients depends mostly on swallowing function and overall management.

MRI ACQUISITION PROTOCOL TO BE USED IN ROUTINE CARE FOR NEURODEGENERATION WITH BRAIN IRON ACCUMULATION PATIENTS

Brain iron accumulation may be visualized with MRI using sequences that are sensitive to metallic content, such as gradient echo T2*-weighted imaging, susceptibility-weighted imaging (SWI) and may be quantified using T2* mapping and quantitative susceptibility mapping (QSM). T2* relaxation times is measured using a number of T2*-weighted images with increasing echo time. T2* relaxation time (and

Table 1. Overview of the main neurodegeneration with brain iron accumulation subtypes

	Gene	Frequency	Inheritance	Onset	Distinctive clinical features	Biological markers
NBIA						
PKAN	*PANK2*	+++	AR	Child Young adult	DP, spasticity, retinopathy Slower progression, psychiatric signs (OCB, S, D)	*Acanthocytosis*
PLAN	*PLA2G6*	+++	AR	Child (INAD) Young adult (ANAD)	Psychomotor regression, spasticity, neuropathy, OA DP, cerebellar ataxia, psychiatric signs	
BPAN	*WDR45*	+++	X-linked	Child DP in early adulthood	Intellectual disability, autism, epilepsy	
MPAN	*C19orf12*	++	AR, AD	Child/young adult	DP, spasticity, dementia, neuropathy, OA	
Aceruloplasminemia	*CP*	+	AR	Adult (40 years)	DP, chorea, cerebellar ataxia, diabetes, retinopathy	*Low CER, high ferritin*
Ferritinopathy	*FTL*	+	AD	Adult (50 years)	DP, chorea, cognitive defects	*Low ferritin*
FAHN	*FA2H*	+	AR	Child/young adult	Spasticity, cerebellar ataxia, DP, CD, epilepsy, OA	
Woodhouse–Sakati	*DCAF17*	+	AR	Adolescent	Intellectual disability, DP, chorea, Alopecia, deafness, hypogonadism, diabetes	
Kufor–Rakeb disease	*ATP13A2* (PARK9)	+	AR	Adolescent	DP, dementia	
CoPAN	*COASY*	+	AR	Child	Intellectual disability, DP, spasticity, paraparesis, psychiatric signs	
NBIA-like						
SCP2	*SCP2*	+	AR	Adult	DP, cerebellar ataxia, neuropathy	
GM1 gangliosidosis	*GLB1*	+	AR	Child	DP, cerebellar ataxia	
AP4-deficiency	*AP4M1*	+	AR	Child	Intellectual disability, microcephaly, spasticity,	
DDHD1	*DDHD1*	+	AR	Child/adult	Spasticity, cerebellar ataxia, neuropathy, retinopathy	
GTPBP2	*GTPBP2*	+	AR	Child	Intellectual disability	

AD, autosomal dominant; ANAD, atypical neuroaxonal dystrophy; AR, autosomal recessive; BPAN, beta-propeller protein-associated neurodegeneration; CER, ceruloplasminemia; CoPAN, coenzyme A synthase protein-associated neurodegeneration; D, depression; DP, dystonia–parkinsonism; FAHN, fatty acid 2 hydroxylase-associated neurodegeneration; INAD, infantile neuroaxonal dystrophy; MPAN, mitochondrial membrane protein-associated neurodegeneration; NBIA, neurodegeneration with brain iron accumulation; OA, optic atrophy; OCB, obsessive–compulsive behavior; PKAN, panthotenate kinase-associated neurodegeneration, PLAN, phospholipase A2 group VI-associated neurodegeneration; S, schizophrenia-like psychosis.

hence the relaxation rate $R2^* = 1/T2^*$) is calculated by measuring the exponential signal decay with increasing echo time. Iron accumulation in tissues results in a decrease $T2^*$ and an increase $R2^*$. SWI combines the magnitude and the phase images to enhance the contrast of structures containing molecules with high susceptibility such as iron. The magnetic susceptibility is a measure of how much a material will become magnetized in an applied magnetic field. QSM is calculated using the $T2^*$

magnitude and phase images and provides a measurement of local magnetic susceptibility variations. Because T2* and SWI images are more sensitive to microscopic inhomogeneities of the magnetic field reflecting iron deposition than spin echo T2-weighted images, these sequences should be added to the MRI acquisition protocol used for NBIA diagnosis. This effect increases with the magnetic field and is therefore greater at 3T, and even more at 7T, than at 1.5T. In contrast, T2 and FLAIR images better evaluate white matter changes, gliosis, and cavitation but are much less sensitive to iron deposition. Cavitation is seen as an area of high signal intensity on T2-weighted images and might provide additional diagnosis clues to the genetic diagnosis. Three-dimensional T1-weighted images are added to evaluate brain morphology changes and atrophy. T1-weighted images may also provide interesting information on metallic deposit. For instance, iron or copper bound to molecules such as neuromelanin form paramagnetic complexes that appear hyperintense on T1-weighted images [8]. This effect may explain the high signal intensity observed in the basal ganglia in some NBIA subtypes [9,10]. Studies have used R2* mapping, mostly in deferiprone trials [6▪,11–13], or QSM [14,15▪] to quantify iron deposition. Importantly, a CT scan shall be performed to look for brain calcifications, which MRI aspect is variable and can be difficult to distinguish from iron deposition in routine practice.

IRON DEPOSITION IN THE NORMAL BRAIN

Iron gradually deposits in specific regions of the normal brain and particularly the basal ganglia. Histologically, the structures richest in iron are the globus pallidus and substantia nigra, followed by the red nucleus, putamen, caudate nucleus, dentate nucleus and the subthalamic nucleus [16]. Weaker iron deposition is also observed in the cerebral and cerebellar cortex, nuclei of the thalamus, the mamillary body, and the tectum [16]. MRI shows early age-related increase in globus pallidus and substantia nigra iron levels, which reaches a plateau in early adulthood [17,18]. Using T2-weighted images at 1.5T, iron deposition is first seen in the globus pallidus, followed by the red nucleus and substantia nigra, and then the dentate nucleus. Decreased signal intensity was not seen in these regions in patients less than 10 years old [18]. Using SWI at 1.5T, iron deposition was detected in the globus pallidus in all children and young adults older than 3 years [19]. In the putamen, iron deposited from the posterolateral to the anteromedial areas of the putamen [19]. Iron deposition in the putamen was not seen in normal subjects during the first decade of life whereas all normal subjects older than 20 years of age exhibited a rim of low SWI signal around the putamen called putaminal pencil lining [20]. In the cortex, iron may be detected at 3T using SWI as a fine band of low signal intensity following the contour of the cortex called the cortical pencil lining. At 1.5T, this sign is observed in all subjects older than 50 years [20].

IMAGING ASPECTS IN THE MOST COMMON NEURODEGENERATION WITH BRAIN IRON ACCUMULATION SUBTYPES

A general summary of the different MRI anomalies observed in the different types of NBIA is presented in Table 2.

Panthotenate kinase-associated neurodegeneration

The typical brain MRI aspect of PKAN is characterized by an abnormal central T2/T2* hyperintensity secondary to gliosis and spongiosis of the anteromedial part of the globus pallidus that is surrounded by a low signal intensity caused by iron accumulation. This pattern is referred to as the 'eye of the tiger' sign and is observed in almost all PKAN patients (Fig. 1a–d). The central hyperintensity can predate the surrounding hypointensity in some patients [21,22▪]. In addition, the hyperintense center may vary in shape over the disease course from small round to streak, and rare patient can eventually have a more homogeneous hypointensity of the globus pallidus [22▪,23]. This is likely because of further accumulation of iron eventually obscuring the central hyperintensity. Associated hypointensity can be observed frequently in the substantia nigra and more rarely in the subthalamic nucleus and the dentate nuclei [22▪,24]. Finally, it is important to keep in mind that bipallidal calcifications can be observed in PKAN [25], and can even be the first neuradiological abnormality [26].

Phospholipase A2 group VI-associated neurodegeneration

PLAN constitutes two forms of infantile neuroaxonal dystrophy (INAD) and atypical neuroaxonal dystrophy (ANAD). Brain MRI shows iron deposits in the globus pallidus, the substantia nigra and the dentate nucleus [24,27,28] but not in all patients [29▪] (Fig. 1e–h). Cerebellar atrophy is constant, affecting both the vermis and hemispheres, and T2/FLAIR hyperintensity of the cerebellar cortex and dentate nuclei are often present [29▪]. The dentate nucleus may be hypointense on T2*-weighted

1350-7540 Copyright © 2020 The Author(s). Published by Wolters Kluwer Health, Inc.

Table 2. MRI features in neurodegeneration with brain iron accumulation

	Areas of iron deposition	Other distinctive features
NBIA		
PKAN	GP (eye of tiger sign), less often SN > DN	Calcifications possible
PLAN	GP, more variably SN, DN	Atrophy/hyperT2 cerebellum Brain atrophy, WM changes
BPAN	GP, SN	HyperT1 rim around SN
MPAN	GP (IML visible), SN	HyperT1 in CN-PU Cortex–cerebellar atrophy
Aceruloplasminemia	GP, RN, PU, CN, Tha, RN, DN, Ctx	
Ferritinopathy	GP, RN, PU, CN, Tha, RN, DN, Ctx Eye of tiger sign possible	Cavitation
FAHN	GP	WM changes, thinning CC Pontocerebellar atrophy
Woodhouse–Sakati	GP, SN	WM changes
Kufor–Rakeb disease	GP, PU, CN	
CoPAN	GP (eye of tiger sign like), SN	Striatal hyper T2, calcification
NBIA-like		
SCP2	GP, SN, RN, DN	Hyper T2 in Tha, pons, WM
GM1 gangliosidosis	GP (wishbone sign) Progression to SN, RN, STN	Hyper T2 in posterior PU
AP4-deficiency	GP	Ventricular enlargement
DDHD1	GP	Thinning CC
GTPBP2	GP, SN	Vermian atrophy

BPAN, beta-propeller protein-associated neurodegeneration; CC, corpus callosum; CN, caudate nucleus; CoPAN, coenzyme A synthase protein-associated neurodegeneration; DN, dentate nucleus; FAHN, fatty acid 2 hydroxylase-associated neurodegeneration; GP, globus pallidus; Hyper T1, hypersignal in T1-weighted images; Hyper T2, hypersignal in T2-weighted images; IML, internal medullary laminae; MPAN, mitochondrial membrane protein-associated neurodegeneration; NBIA, neurodegeneration with brain iron accumulation; PKAN, panthotenate kinase-associated neurodegeneration, PLAN, phospholipase A2 group VI-associated neurodegeneration; PU, putamen; RN, red nucleus; SN, substantia nigra; Tha, thalamus; WM, white matter.

images [24,27] or hyperintense on T2-weighted images [29▪]. Cerebellar atrophy is greater when disease onset is earlier [29▪]. Cerebral atrophy and white matter changes may also be observed [29▪,30,31]. Occasionally, the substantia nigra may be more affected than the globus pallidus in some patients [31].

Beta-propeller protein-associated neurodegeneration

Patients with BPAN displays iron deposition in the globus pallidus and substantia nigra on brain MRI [30,32–34] (Fig. 2). In contrast to normal individuals, the putaminal pencil lining was observed early during the first decade of life in BPAN patients [20]. A hyperintense halo has also been reported around the substantia nigra using T1-weighted images [30,32,35,36] but this sign seems inconstant [33]. Brain and hippocampal atrophy as well as cortical thinning have been reported in patients with epileptic encephalopathies [34,36–38]. During early childhood, BPAN patients can present transient hyperintensity and swelling in the globus pallidus and substantia nigra because of infections, followed by elevated iron measured by QSM [39].

Mitochondrial membrane protein-associated neurodegeneration

Brain MRI in MPAN shows iron deposition in the globus pallidus and the substantia nigra (Fig. 3) [40]. Visibility of the internal medullary lamina as a band of high signal intensity in the globus pallidus has been reported [9,15▪,41,42]. Whether this aspect is specific to MPAN remains to be determined. Additional T1 hyperintensity [9], SWI hypointensity [43,44] and susceptibility increase [15▪] was reported in the caudate nucleus and putamen. Cortical or cerebellar atrophy was observed after long disease duration [15▪,40]. Autosomal dominant forms of MPAN also exist because of a likely gain of function of certain pathogenic variants in *C19orf12* [45▪▪]. Independent of inheritance pattern, most MPAN cases are phenotypically similar, including the neuroimaging aspects.

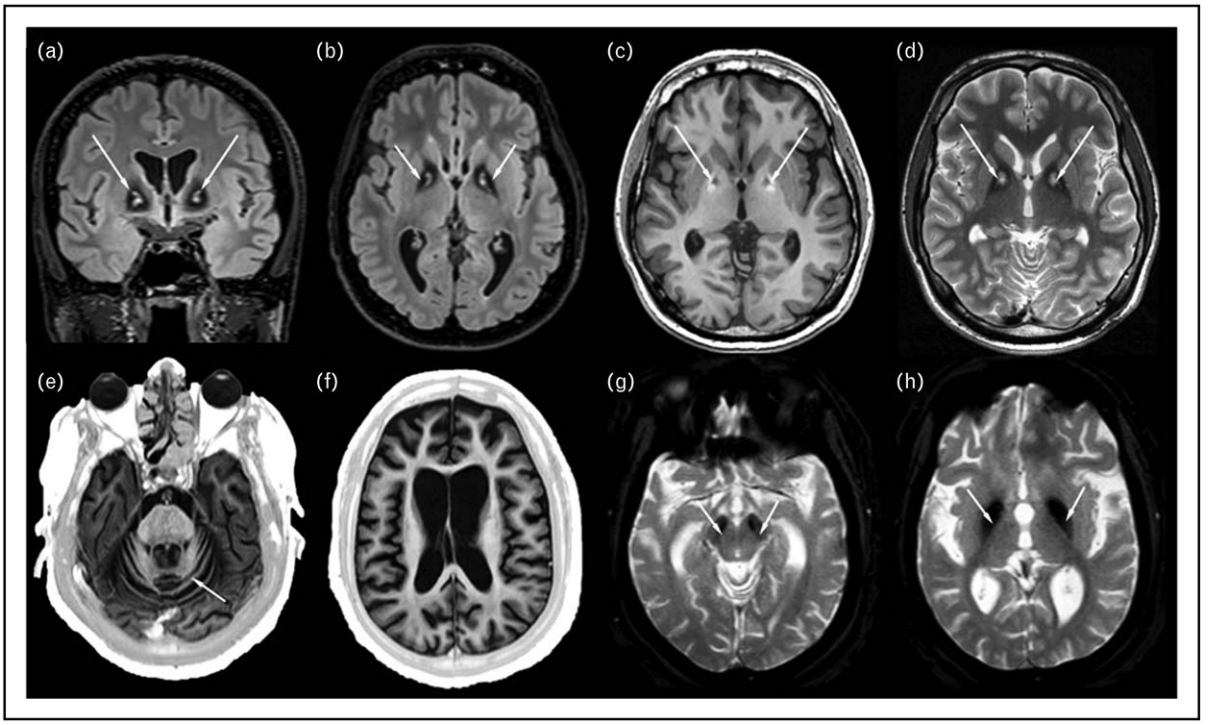

FIGURE 1. Panthotenate kinase-associated neurodegeneration and phospholipase A2 group VI-associated neurodegeneration. (a–d) A 43-year-old male patient with PKAN. Coronal FLAIR (a), axial FLAIR (b), (c) T1-weighted (T1-w), and (d) T2-weighted (T2-w) images. The FLAIR and T2-w images show abnormal signal intensity in bilateral globus pallidus with central hyperintensiy (probably because of gliosis) and peripheral rim of hypointensity (because of iron deposition) corresponding to the eye of the tiger sign (arrows). The T1-w image shows central hypointenisy surrounded by a rim of high signal intensity probably because of the presence of paramagnetic material (arrows). (e–h) A 30-year-old female patient with PLAN. Axial T1-weighted (T1-w, e and f) and T2*-weighted images (T2*-w, g and h). Images show cerebellar atrophy (arrow in e), brain atrophy with ventricular enlargement (f) and signal hypointensity indicating iron deposition (arrows) in bilateral substantia nigra (g) and globus pallidus (h). PKAN, panthotenate kinase-associated neurodegeneration, PLAN, phospholipase A2 group VI-associated neurodegeneration.

IMAGING ASPECTS IN IRON HOMEOSTASIS-ASSOCIATED NEURODEGENERATION WITH BRAIN IRON ACCUMULATION

Aceruloplasminemia

Brain MRI in patients with aceruloplasminemia showed diffuse iron deposits involving all basal ganglia (globus pallidus, striatum, substantia nigra), the red nucleus, the dentate nucleus and the thalamus, the mammillary bodies, the lateral habenula, the hippocampus and the cortex [11,14,27,46–48] (Fig. 4a–d). It should be noted that patients with hypoceruloplasminemia, that is, bearing one heterozygous pathogenic *CP* variant, may be symptomatic and present with pallidal hypointensity, cerebral white matter hyperintensity, and cerebellar atrophy [49].

Neuroferritinopathy

Brain MRI shows diffuse variable iron deposition in the globus pallidus, putamen, dentate nuclei, and in some patients in caudate nuclei and thalami (Fig. 4e–h). An eye of the tiger sign may be observed [24]. In about half of the subjects, cavitations or cystic degeneration are seen as confluent areas of T2/FLAIR hyperintensity involving the globus pallidus and putamen [24,50–52]. Iron deposition is also observed in the cortex, a sign described as 'cortical pencil lining' [53]. This sign is also observed in aceruloplasminemia [20]. However, it is also observed in subjects over 50 years of age so that its usefulness from this age is questionable [20].

IMAGING ASPECTS IN ULTRA RARE NEURODEGENERATION WITH BRAIN IRON ACCUMULATION DISORDERS

Fatty acid 2 hydroxylase-associated neurodegeneration

FAHN is remarkable because of the association of T2 hypointensity in the globus pallidus with

1350-7540 Copyright © 2020 The Author(s). Published by Wolters Kluwer Health, Inc.

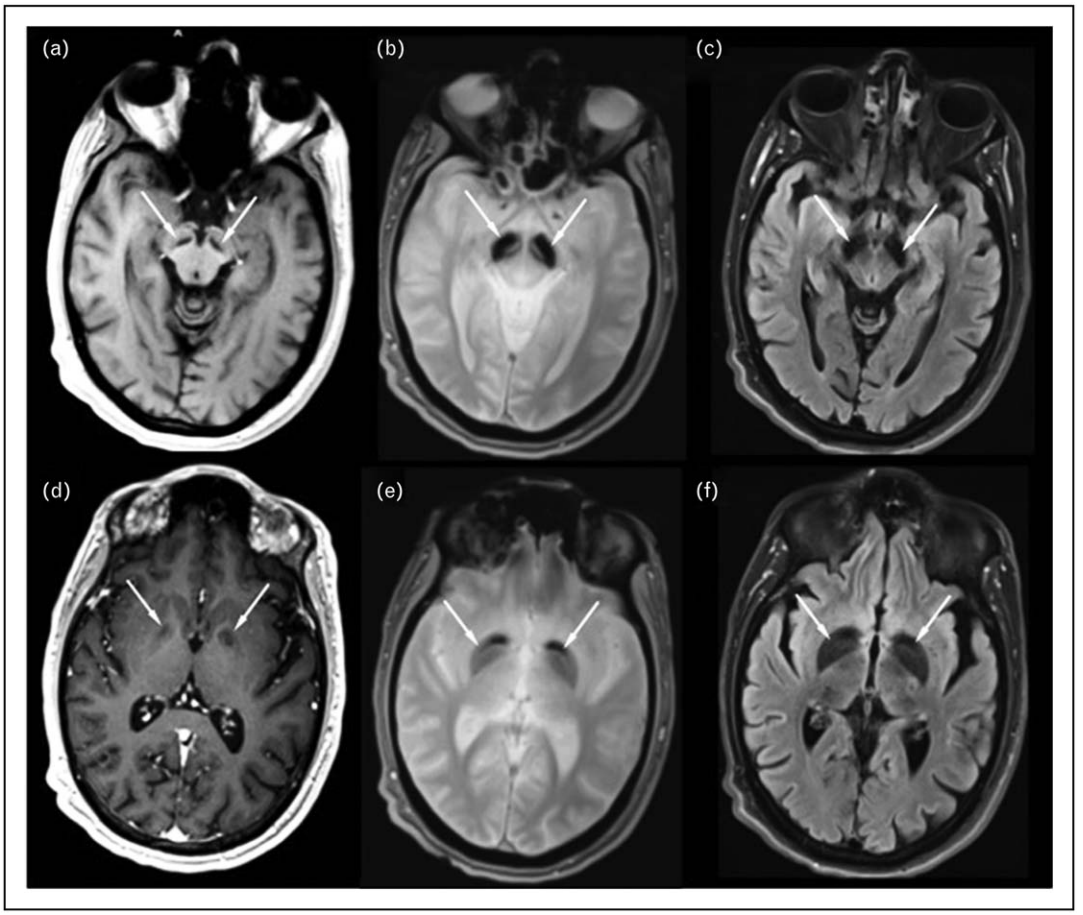

FIGURE 2. Beta-propeller protein-associated neurodegeneration. A 37-year-old male patient. Axial T1-weighted (T1-w, a and d), T2*-weighted (T2*-w, b and e) and FLAIR images (c and f). The SN (arrows) is hypointense on T2*-w (b) and FLAIR (c) images (b), and present a central area of hyposignal surrounded by a rim of high signal intensity on T1-w images (a). The globus pallidus (arrows) is hypointense in all images (d–f).

marked brainstem (pons and medulla oblongata, not observed in PLAN) and cerebellar atrophy, T2/FLAIR white matter hyperintensities, thinning of the corpus callosum, and mild generalized cortical atrophy [54] (Fig. 5a–d). Recently, the acronym WHAT was proposed to highlight this combination of white matter changes, hypointensity of the globus pallidus, pontocerebellar atrophy, and thin corpus callosum [55▪▪].

Woodhouse–Sakati syndrome

Some patients with this syndrome show iron deposition in the globus pallidus on brain MRI and, as disease progresses, in the substantia nigra and red nucleus [56,57▪] (Fig. 5e–h). Other findings are iron deposition in a small pituitary gland, leukodystrophy and more rarely prominent perivascular spaces and restricted diffusion in the splenium of the corpus callosum [57▪,58].

Kufor–Rakeb disease

In Kufor–Rakeb disease, brain MRI can show iron deposition in the basal ganglia (caudate and lenticular nucleus) and brain atrophy [59–61] (Supplementary Fig. 1, http://links.lww.com/CONR/A52), although this abnormality is inconstant [62].

Coenzyme A synthase protein-associated neurodegeneration

Brain MRI in CoPAN typically shows swollen striatum and thalamus, hyperintense in T2-weighted images in early childhood that may regress over time and later iron deposition in the globus pallidus and substantia nigra [63,64] (Supplementary Fig. 1, http://links.lww.com/CONR/A52). The early striatal and thalamic changes might thus occur before the increase of pallidal iron content that was observed between 7 and 9 years [63,64]. Pallidal changes can mimic the 'eye-of-the-tiger' sign seen in PKAN because of pallidal calcifications [64].

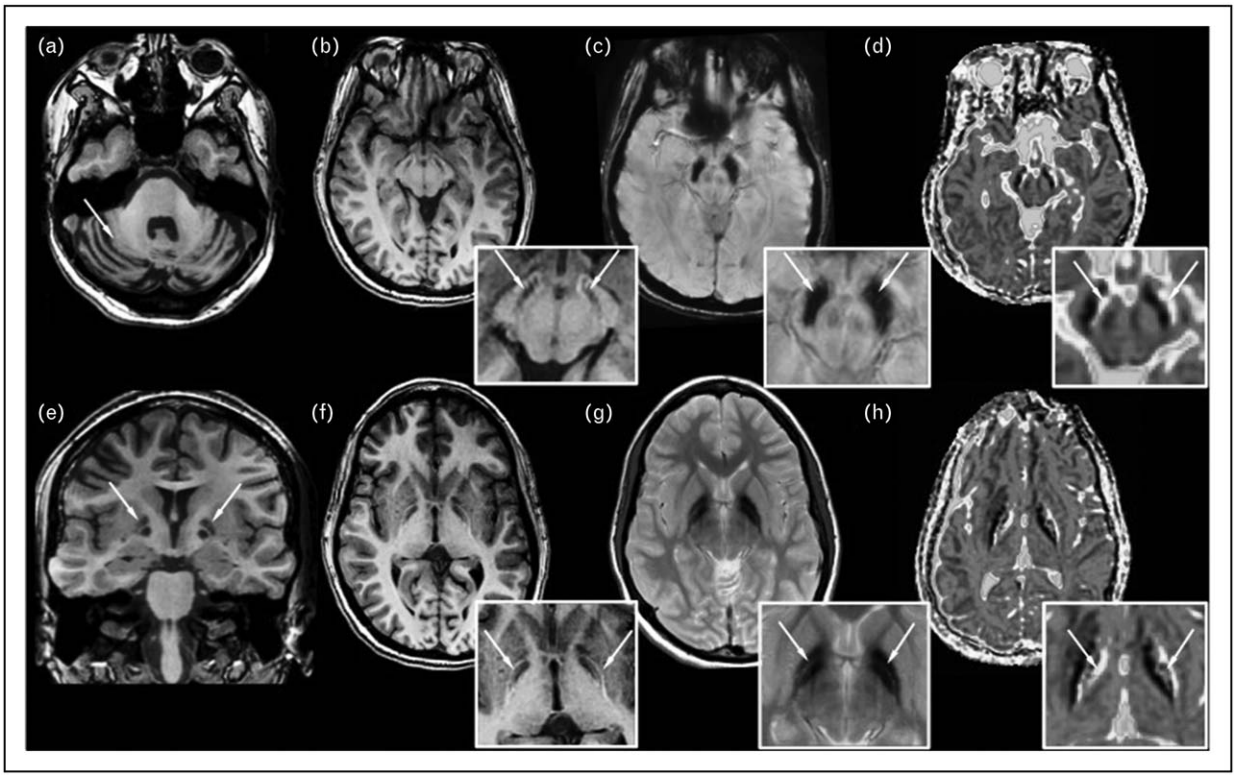

FIGURE 3. Mitochondrial membrane protein-associated neurodegeneration. A 26-year-old female patient. Axial images passing at the level of the cerebellum (a), the substantia nigra (b-d), coronal (e) and axial images passing at the level of lenticular nucleus (f–h). Images are T1-weighted (a, b, e, f), T2*-weighted (c and g) and ADC maps (d and h). Boxes show enlargement of the substantia nigra (b–d) and the lenticular nucleus (f–h). Images show cerebellar atrophy (arrow in a). The SN (b–d) and the globus pallidus (f–h) are hypointense on T2*-w images, present a central area of hyposignal surrounded by a rim of high signal intensity on T1-w images and show areas of increased apparent diffusion coefficient (ADC) probably because of gliosis (arrows). The internal medullary laminae is clearly visible in g (arrows).

OTHER ENTITIES THAT MAY PRESENT WITH A NEURODEGENERATION WITH BRAIN IRON ACCUMULATION PATTERN

Other rare genetic diseases occur in young patients with slowly progressive generalized dystonia-parkinsonism and an accumulation of iron in the basal ganglia visible on MRI. Whether they belong to NBIA or are NBIA-like diseases is debated, however.

SCPx syndrome

Brain MRI in a 51-year-old man and a 44-year-old man with *SCP2* pathogenic variants showed bilateral T2/FLAIR hyperintense signals in the thalamus, the pons, and the occipital region [65,66] and reduced SWI signal in the globus pallidus, substantia nigra, red nuclei, and dentate nuclei [66] (Supplementary Fig. 1, http://links.lww.com/CONR/A52).

GM1 type3 gangliosidosis

Reduced SWI signal because of iron deposition was observed in the globus pallidus with progression to the substantia nigra, the red nucleus and the subthalamic nucleus [67,68] (Supplementary Fig. 1, http://links.lww.com/CONR/A52). The aspect of the globus pallidus was particular with a marked drop in signal intensity of the external and internal parts of the pallidum separated by the hypersignal of the internal medullary lamina reminiscent of that of a wishbone [67]. T2 and FLAIR hyperintensity was present in the posterior putamen and posterior white matter [67]. The combination of the wishbone sign and the posterior putaminal hyperintensity is highly suggestive of this disorder.

AP4 deficiency

In three patients aged 16 to 23 years with biallelic *AP4M1* pathogenic variants brain MRI showed global brain atrophy, white matter loss, ventricular enlargement, thinning of the splenium of the corpus callosum and SWI hypointensity in the globus pallidus [69] (Supplementary Fig. 1, http://links.lww.com/CONR/A52). Likewise, a 13-year-old

1350-7540 Copyright © 2020 The Author(s). Published by Wolters Kluwer Health, Inc.

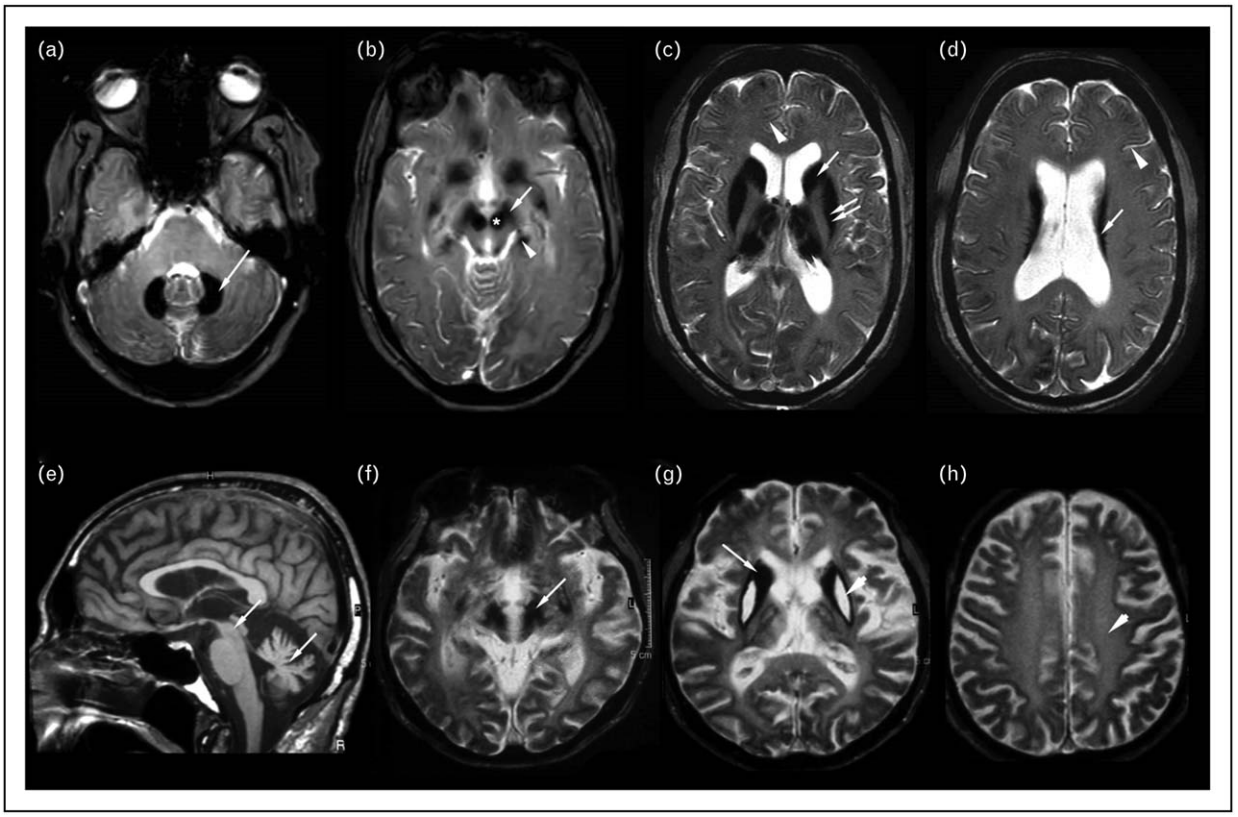

FIGURE 4. Aceruloplasminemia and neuroferritinopathy. (a–d) A 60-year-old female patient with aceruloplasminemia after 7 years of disease duration. Axial T2*-weighted images showing widespread areas of hyposignal because of iron deposition in (a) the dentate nuclei (arrow), (b) the hippocampus (arrowhead), red nucleus (asterisk) and substantia nigra (arrow), (c) the caudate nucleus (arrow) and putamen (double arrows), the thalamus (double arrowheads), and the cortex (arrowhead), (d) the caudate nucleus (arrow) and the cortex (Image courtesy T. Tourdias). (e–h) A 62-year-old male patient with neuroferritinopathy after 12 years of disease duration. (e) Sagittal T1-weighted images showing cerebellar and midbrain atrophy (arrows), (f–h) Axial T2-weighted images showing (f) widespread areas of hyposignal because of iron deposition in the midbrain and substantia nigra (arrow), (g) the globus pallidus, caudate nucleus, thalamus and putamen (arrow) with areas of high signal intensity in the putamen corresponding to cavitation (arrowhead), (h) white matter hyperintensities (arrowhead).

girl with a homozygous pathogenic variant in *AP4S1* had hypointensity in the globus pallidus and thinning of the splenium of the corpus callosum [70].

DDHD1 pathogenic variants

Brain MRI in a 55-year-old man showed T2 hyposignal in the globus pallidus, T2 hypersignal of the supratentorial white matter and thinning of the corpus callosum [71].

GTPBP2 pathogenic variants

Brain MRI in three patients aged 29–34 years (two males, one female) showed reduced signal on SWI in the globus pallidus and substantia nigra and vermian atrophy [72].

CONCLUSION

Brain MRI using iron-sensitive MRI sequences is crucial for the diagnosis of NBIA by showing iron deposits in the basal ganglia, mostly the globus pallidus and substantia nigra. Some subtypes also show characteristic or additional MRI changes: the 'eye of the tiger 'sign in PKAN and a similar pattern reported in some patients with CoPAN and neuroferritinopathies, widespread iron deposition in the basal ganglia, thalamus, dentate nucleus and red nucleus in aceruloplasminemia and neuroferritinopathy, cavitation in neuroferritinopathy, white matter abnormalities in FAHN, Woodhouse–Sakati and SCPx syndromes, cerebellar atrophy in PLAN, thinning of corpus callosum and pontocerebellar atrophy in FAHN, swollen striatum with T2 hyperintensity in CoPAN.

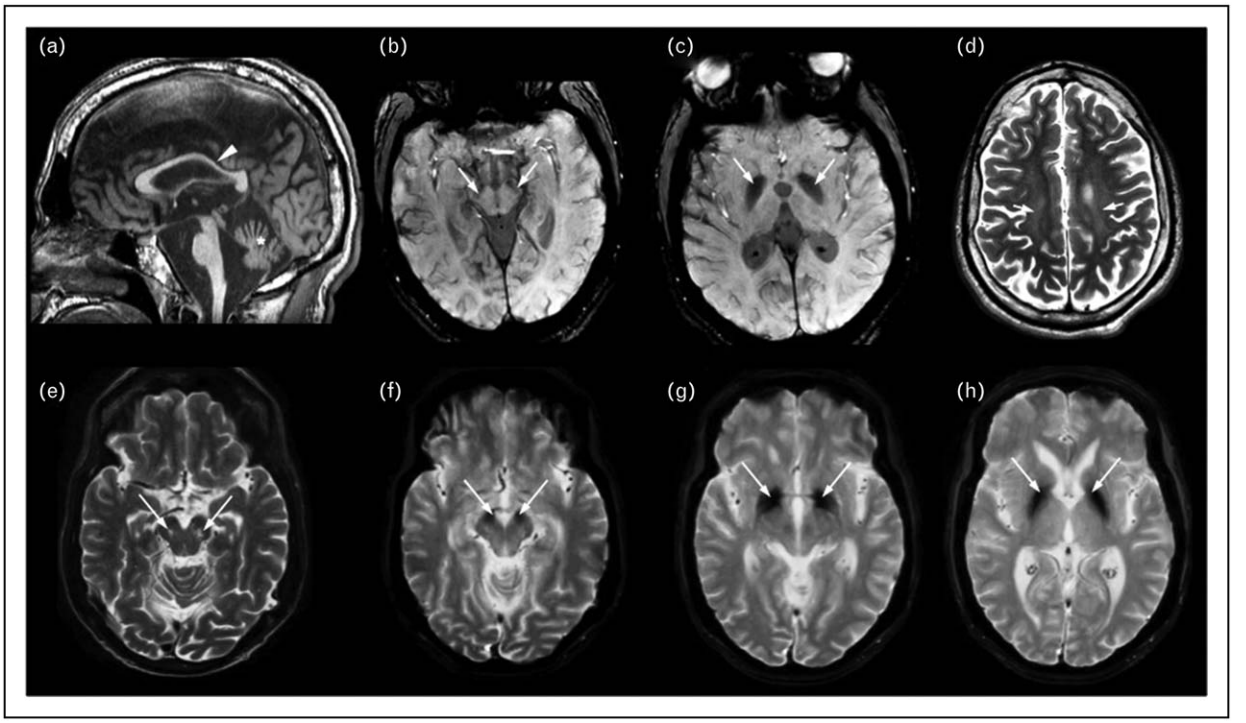

FIGURE 5. FAHN and Woodhouse–Sakati syndrome. (a–d) A 29-year-old male patient with FAHN. (a) Sagittal T1-weighted image showing cerebellar (asterisk) and brainstem atrophy and thinning of the corpus callosum (arrow). (b and c) Axial SWI images showing hyposignal indicating iron deposition (arrows) in the substantia nigra (b), and the globus pallidus (c). (d) Axial T2-weighted image showing hypersignal in the white matter (double arrows). (e–h) Patient with Woodhouse–Sakati syndrome. (e) Axial T2-weighted and (f–h) T2*-weighted images showing (e) enlarged perivascular spaces in the area of the substantia nigra (arrow) and hyposignal indicating iron deposition (arrows) in the substantia nigra (f), and the globus pallidus (g and h).

An important limitation of imaging to date is that examinations were carried out with different magnetic fields, different sequences not always comparable on small series of patients. Few quantitative studies of iron deposition have been published. This makes it difficult to study the specificity of the signal anomalies observed (such as the T1 hypersignal rim, the wishbone sign), the relative importance of iron load between the diseases and the involvement of the different regions (external and internal globus pallidus, internal medullary laminae, substantia nigra, dentate nucleus, subthalamic nucleus). Future studies using quantitative MRI, high resolution at 3T may help to better detect and quantify iron deposition in NBIA and to determine whether iron content correlates with clinical signs and disease prognosis and evolution.

Acknowledgements

We thank Drs. François Chalard, Denis Lacroix, Delphine Leclercq and Thomas Tourdias, who contributed to image acquisition and Patricia Maurin for molecular analyses of several patients whose images are presented in the figures.

Financial support and sponsorship

None.

Conflicts of interest

There are no conflicts of interest.

REFERENCES AND RECOMMENDED READING

Papers of particular interest, published within the annual period of review, have been highlighted as:

- ■ of special interest
- ■■ of outstanding interest

1. Hayflick SJ, Kurian MA, Hogarth P. Neurodegeneration with brain iron ■■ accumulation. Handb Clin Neurol 2018; 147:293–305.

This article is a recent, comprehensive and well written review detailing all aspects of NBIA.

2. Di Meo I, Tiranti V. Classification and molecular pathogenesis of NBIA ■■ syndromes. Eur J Paediatr Neurol 2018; 22:272–284.

This article provides an interesting review of the molecular pathogenesis of NBIA.

3. Masaldan S, Bush AI, Devos D, *et al.* Striking while the iron is hot: Iron ■■ metabolism and ferroptosis in neurodegeneration. Free Radic Biol Med 2019; 133:221–233.

This thorough review on iron and neurodegeneration decipher the potential mechanism of iron-dependent programmed cell death. It also investigates ferroptosis in neurodegenerative disease and how it can be a therapeutic target.

4. Macerollo A, Perry R, Stamelou M, *et al.* Susceptibility-weighted imaging changes suggesting brain iron accumulation in Huntington's disease: an epiphenomenon which causes diagnostic difficulty. Eur J Neurol 2014; 21:e16–e17.

1350-7540 Copyright © 2020 The Author(s). Published by Wolters Kluwer Health, Inc.

5. Timmermann L, Pauls KA, Wieland K, *et al.* Dystonia in neurodegeneration with brain iron accumulation: outcome of bilateral pallidal stimulation. Brain 2010; 133:701–712.
6. ■ Klopstock T, Tricta F, Neumayr L, *et al.* Safety and efficacy of deferiprone for pantothenate kinase-associated neurodegeneration: a randomised, double-blind, controlled trial and an open-label extension study. Lancet Neurol 2019; 18:631–642.

This is an 18-month, randomised, double-blind, placebo-controlled trial, followed by a preplanned 18-month, open-label extension study, that assessed whether the iron chelator deferiprone can reduce brain iron and slow disease progression in patients with PKAN. Deferiprone was well tolerated and seemed somewhat slowed disease progression although not significantly. R^{2*} measurements for iron concentrations in the globus pallidus was unchanged in the placebo group whereas there was a significant decrease in the deferiprone group.

7. Jeong S, Hogarth P, Placzek A, *et al.* 4'-phosphopantetheine corrects CoA, iron, and dopamine metabolic defects in mammalian models of PKAN. EMBO Mol Med 2019; 11:e10489.
8. Sulzer D, Cassidy C, Horga G, *et al.* Neuromelanin detection by magnetic resonance imaging (MRI) and its promise as a biomarker for Parkinson's disease. NPJ Parkinsons Dis 2018; 4:11.
9. Schulte EC, Claussen MC, Jochim A, *et al.* Mitochondrial membrane protein associated neurodegenration: a novel variant of neurodegeneration with brain iron accumulation. Mov Disord 2013; 28:224–227.
10. Hayflick SJ, Kruer MC, Gregory A, *et al.* beta-Propeller protein-associated neurodegeneration: a new X-linked dominant disorder with brain iron accumulation. Brain 2013; 136:1708–1717.
11. Pan PL, Tang HH, Chen Q, *et al.* Desferrioxamine treatment of aceruloplasminemia: long-term follow-up. Mov Disord 2011; 26:2142–2144.
12. Cossu G, Abbruzzese G, Matta G, *et al.* Efficacy and safety of deferiprone for the treatment of pantothenate kinase-associated neurodegeneration (PKAN) and neurodegeneration with brain iron accumulation (NBIA): results from a four years follow-up. Parkinsonism Relat Disord 2014; 20:651–654.
13. Zorzi G, Zibordi F, Chiapparini L, *et al.* Iron-related MRI images in patients with pantothenate kinase-associated neurodegeneration (PKAN) treated with deferiprone: results of a phase II pilot trial. Mov Disord 2011; 26:1756–1759.
14. Zhou L, Chen Y, Li Y, *et al.* Intracranial iron distribution and quantification in aceruloplasminemia: a case study. Magn Reson Imaging 2020; 70:29–35.
15. ■ Dusek P, Mekle R, Skowronska M, *et al.* Brain iron and metabolic abnormalities in C19orf12 mutation carriers: a 7.0 tesla MRI study in mitochondrial membrane protein-associated neurodegeneration. Mov Disord 2020; 35:142–150.

This 7T study quantified magnetic susceptibility in MPAN patient and nonmanifesting heterozygous carriers. Susceptibility was increased in the globus pallidus and substantia nigra and the caudate nucleus. Nonmanifesting carriers had increased magnetic susceptibility in the putamen and caudate nucleus, which may be an endophenotypic marker of genetic heterozygosity.

16. Hallgren B, Sourander P. The effect of age on the nonhaemin iron in the human brain. J Neurochem 1958; 3:41–51.
17. Aquino D, Bizzi A, Grisoli M, *et al.* Age-related iron deposition in the basal ganglia: quantitative analysis in healthy subjects. Radiology 2009; 252:165–172.
18. Aoki S, Okada Y, Nishimura K, *et al.* Normal deposition of brain iron in childhood and adolescence: MR imaging at 1.5 T. Radiology 1989; 172:381–385.
19. Harder SL, Hopp KM, Ward H, *et al.* Mineralization of the deep gray matter with age: a retrospective review with susceptibility-weighted MR imaging. AJNR Am J Neuroradiol 2008; 29:176–183.
20. van der Weijden MCM, van Laar PJ, Lambrechts RA, *et al.* Cortical pencil lining on SWI MRI in NBIA and healthy aging. BMC Neurol 2019; 19:233.
21. Hayflick SJ, Hartman M, Coryell J, *et al.* Brain MRI in neurodegeneration with brain iron accumulation with and without PANK2 mutations. AJNR Am J Neuroradiol 2006; 27:1230–1233.
22. ■ Lee JH, Gregory A, Hogarth P, *et al.* Looking deep into the eye-of-the-tiger in pantothenate kinase-associated neurodegeneration. AJNR Am J Neuroradiol 2018; 39:583–588.

This article describes the T2-weighted and SWI signal changes at 3T and 7T in a large series of patients with pathogenic variants in *PANK2*. Changes were observed in the globus pallidus that progressed from medial to lateral parts of the nucleus with increasing age, the subthalamic nucleus, the substantia nigra and in the nigro-pallido-striatal fiber tract.

23. Delgado RF, Sanchez PR, Speckter H, *et al.* Missense PANK2 mutation without 'eye of the tiger' sign: MR findings in a large group of patients with pantothenate kinase-associated neurodegeneration (PKAN). J Magn Reson Imaging 2012; 35:788–794.
24. McNeill A, Birchall D, Hayflick SJ, *et al.* $T2^*$ and FSE MRI distinguishes four subtypes of neurodegeneration with brain iron accumulation. Neurology 2008; 70:1614–1619.
25. Fasano A, Shahidi G, Lang AE, Rohani M. Basal ganglia calcification in a case of PKAN. Parkinsonism Relat Disord 2017; 36:98–99.
26. Wu YW, Hess CP, Singhal NS, *et al.* Idiopathic basal ganglia calcifications: an atypical presentation of PKAN. Pediatr Neurol 2013; 49:351–354.
27. Salomao RP, Pedroso JL, Gama MT, *et al.* A diagnostic approach for neurodegeneration with brain iron accumulation: clinical features, genetics and brain imaging. Arq Neuropsiquiatr 2016; 74:587–596.
28. Kurian MA, Morgan NV, MacPherson L, *et al.* Phenotypic spectrum of neurodegeneration associated with mutations in the PLA2G6 gene (PLAN). Neurology 2008; 70:1623–1629.
29. ■ Darling A, Aguilera-Albesa S, Tello CA, *et al.* PLA2G6-associated neurodegeneration: new insights into brain abnormalities and disease progression. Parkinsonism Relat Disord 2019; 61:179–186.

Sixteen patients with PLAN were genotyped, evaluated using a standardized neurological examination, and had qualitative and quantitative assessment of brain MRI abnormalities.

30. Amaral LL, Gaddikeri S, Chapman PR, *et al.* Neurodegeneration with brain iron accumulation: clinicoradiological approach to diagnosis. J Neuroimaging 2015; 25:539–551.
31. Malaguti MC, Melzi V, Di Giacopo R, *et al.* A novel homozygous PLA2G6 mutation causes dystonia-parkinsonism. Parkinsonism Relat Disord 2015; 21:337–339.
32. Haack TB, Hogarth P, Gregory A, *et al.* BPAN: the only X-linked dominant NBIA disorder. Int Rev Neurobiol 2013; 110:85–90.
33. Uchino S, Saitsu H, Kumada S, *et al.* Stereotypic hand movements in beta-propeller protein-associated neurodegeneration: first video report. Mov Disord Clin Pract 2015; 2:190–191.
34. Carvill GL, Liu A, Mandelstam S, *et al.* Severe infantile onset developmental and epileptic encephalopathy caused by mutations in autophagy gene WDR45. Epilepsia 2018; 59:e5–e13.
35. Wynn DP, Pulst SM. A novel WDR45 mutation in a patient with beta-propeller protein-associated neurodegeneration. Neurol Genet 2017; 3:e124.
36. Ichinose Y, Miwa M, Onohara A, *et al.* Characteristic MRI findings in beta-propeller protein-associated neurodegeneration (BPAN). Neurol Clin Pract 2014; 4:175–177.
37. Russo C, Ardissone A, Freri E, *et al.* Substantia nigra swelling and dentate nucleus T2 hyperintensity may be early magnetic resonance imaging signs of beta-propeller protein-associated neurodegeneration. Mov Disord Clin Pract 2019; 6:51–56.
38. Hattingen E, Handke N, Cremer K, *et al.* Clinical and imaging presentation of a patient with beta-propeller protein-associated neurodegeneration, a rare and sporadic form of neurodegeneration with brain iron accumulation (NBIA). Clin Neuroradiol 2017; 27:481–483.
39. Ishiyama A, Kimura Y, Iida A, *et al.* Transient swelling in the globus pallidus and substantia nigra in childhood suggests SENDA/BPAN. Neurology 2018; 90:974–976.
40. Hartig MB, Iuso A, Haack T, *et al.* Absence of an orphan mitochondrial protein, c19orf12, causes a distinct clinical subtype of neurodegeneration with brain iron accumulation. Am J Hum Genet 2011; 89:543–550.
41. Skowronska M, Kmiec T, Czlonkowska A, Kurkowska-Jastrzebska I. Transcranial sonography in mitochondrial membrane protein-associated neurodegeneration. Clin Neuroradiol 2018; 28:385–392.
42. Olgiati S, Dogu O, Tufekcioglu Z, *et al.* The p.Thr11Met mutation in c19orf12 is frequent among adult Turkish patients with MPAN. Parkinsonism Relat Disord 2017; 39:64–70.
43. Alavi A, Mokhtari M, Hajati R, *et al.* Late-onset mitochondrial membrane protein-associated neurodegeneration with extensive brain iron deposition. Mov Disord Clin Pract 2020; 7:120–121.
44. Gore E, Appleby BS, Cohen ML, *et al.* Clinical and imaging characteristics of late onset mitochondrial membrane protein-associated neurodegeneration (MPAN). Neurocase 2016; 22:476–483.
45. ■■ Gregory A, Lotia M, Jeong SY, *et al.* Autosomal dominant mitochondrial membrane protein-associated neurodegeneration (MPAN). Mol Genet Genomic Med 2019; 7:e00736.

The article presents evidence of autosomal dominant MPAN and proposes a mechanism to explain these cases. The clinical, genetic, neuropathology and imaging findings are described. The authors demonstrate that MPAN can manifest as a result of only one pathogenic *C19orf12* variant.

46. Fasano A, Colosimo C, Miyajima H, *et al.* Aceruloplasminemia: a novel mutation in a family with marked phenotypic variability. Mov Disord 2008; 23:751–755.
47. Rusticeanu M, Zimmer V, Schleithoff L, *et al.* Novel ceruloplasmin mutation causing aceruloplasminemia with hepatic iron overload and diabetes without neurological symptoms. Clin Genet 2014; 85:300–301.
48. Stelten BML, van Ommen W, Keizer K. Neurodegeneration with brain iron accumulation: a novel mutation in the ceruloplasmin gene. JAMA Neurol 2019; 76:229–230.
49. Jimenez-Huete A, Bernar J, Miyajima H, *et al.* Multiple motor system dysfunction associated with a heterozygous ceruloplasmin gene mutation. J Neurol 2008; 255:1083–1084.
50. Devos D, Tchofo PJ, Vuillaume I, *et al.* Clinical features and natural history of neuroferritinopathy caused by the 458dupA FTL mutation. Brain 2009; 132(Pt 6):e109.
51. Nishida K, Garringer HJ, Futamura N, *et al.* A novel ferritin light chain mutation in neuroferritinopathy with an atypical presentation. J Neurol Sci 2014; 342:173–177.
52. Ohta E, Takiyama Y. MRI findings in neuroferritinopathy. Neurol Res Int 2012; 2012:197438.
53. Batla A, Adams ME, Erro R, *et al.* Cortical pencil lining in neuroferritinopathy: a diagnostic clue. Neurology 2015; 84:1816–1818.

54. Kruer MC, Paisan-Ruiz C, Boddaert N, *et al.* Defective FA2H leads to a novel form of neurodegeneration with brain iron accumulation (NBIA). Ann Neurol 2010; 68:611–618.
55. Rattay TW, Lindig T, Baets J, *et al.* FAHN/SPG35: a narrow phenotypic ■■ spectrum across disease classifications. Brain 2019; 142:1561–1572.
The authors performed an in-depth clinical and retrospective neurophysiological and imaging study in a cohort of 19 cases with biallelic *FA2H* pathogenic variants.
56. Louro P, Duraes J, Oliveira D, *et al.* Woodhouse-Sakati syndrome: first report of a Portuguese case. Am J Med Genet A 2019; 179:2237–2240.
57. Abusrair AH, Bohlega S, Al-Semari A, *et al.* Brain MR imaging findings in ■ Woodhouse-Sakati syndrome. AJNR Am J Neuroradiol 2018; 39:2256–2262.
This article reports the brain MRI findings in 26 patients with Woodhouse–Sakati syndrome.
58. Sendur SN, Oguz S, Utine GE, *et al.* A case of Woodhouse-Sakati syndrome with pituitary iron deposition, cardiac and intestinal anomalies, with a novel mutation in DCAF17. Eur J Med Genet 2019; 62:103687.
59. Behrens MI, Bruggemann N, Chana P, *et al.* Clinical spectrum of Kufor-Rakeb syndrome in the Chilean kindred with ATP13A2 mutations. Mov Disord 2010; 25:1929–1937.
60. Schneider SA, Paisan-Ruiz C, Quinn NP, *et al.* ATP13A2 mutations (PARK9) cause neurodegeneration with brain iron accumulation. Mov Disord 2010; 25:979–984.
61. Bruggemann N, Hagenah J, Reetz K, *et al.* Recessively inherited parkinsonism: effect of ATP13A2 mutations on the clinical and neuroimaging phenotype. Arch Neurol 2010; 67:1357–1363.
62. Williams DR, Hadeed A, al-Din AS, *et al.* Kufor Rakeb disease: autosomal recessive, levodopa-responsive parkinsonism with pyramidal degeneration, supranuclear gaze palsy, and dementia. Mov Disord 2005; 20:1264–1271.
63. Evers C, Kaufmann L, Seitz A, *et al.* Exome sequencing reveals a novel CWF19L1 mutation associated with intellectual disability and cerebellar atrophy. Am J Med Genet A 2016; 170:1502–1509.
64. Dusi S, Valletta L, Haack TB, *et al.* Exome sequence reveals mutations in CoA synthase as a cause of neurodegeneration with brain iron accumulation. Am J Hum Genet 2014; 94:11–22.
65. Ferdinandusse S, Kostopoulos P, Denis S, *et al.* Mutations in the gene encoding peroxisomal sterol carrier protein X (SCPx) cause leukencephalopathy with dystonia and motor neuropathy. Am J Hum Genet 2006; 78:1046–1052.
66. Horvath R, Lewis-Smith D, Douroudis K, *et al.* SCP2 mutations and neurodegeneration with brain iron accumulation. Neurology 2015; 85:1909–1911.
67. Hajirnis O, Udwadia-Hegde A. Chronic GM1 gangliosidosis with characteristic 'wish bone sign' on brain MRI. Another type of neurodegeneration with brain iron accumulation? Mov Disord Clin Pract 2015; 2:323–325.
68. Roze E, Paschke E, Lopez N, *et al.* Dystonia and parkinsonism in GM1 type 3 gangliosidosis. Mov Disord 2005; 20:1366–1369.
69. Roubertie A, Hieu N, Roux CJ, *et al.* AP4 deficiency: a novel form of neurodegeneration with brain iron accumulation? Neurol Genet 2018; 4:e217.
70. Vill K, Muller-Felber W, Alhaddad B, *et al.* A homozygous splice variant in AP4S1 mimicking neurodegeneration with brain iron accumulation. Mov Disord 2017; 32:797–799.
71. Dard R, Meyniel C, Touitou V, *et al.* Mutations in DDHD1, encoding a phospholipase A1, is a novel cause of retinopathy and neurodegeneration with brain iron accumulation. Eur J Med Genet 2017; 60:639–642.
72. Jaberi E, Rohani M, Shahidi GA, *et al.* Identification of mutation in GTPBP2 in patients of a family with neurodegeneration accompanied by iron deposition in the brain. Neurobiol Aging 2016; 38:216.e11–216.e18.

1350-7540 Copyright © 2020 The Author(s). Published by Wolters Kluwer Health, Inc.